WAVE MODE COUPLING AND INSTABILITY IN THE INTERNAL WAVE IN ALUMINUM REDUCTION CELLS

Nobuo Urata
Consultant, 770 Cascade Drive Sunnyvale CA 94087

Keywords: aluminum, reduction, instability, wave, MHD

Abstract

In aluminum reduction cells, the interfacial surface wave causes uneven anode-cathode distance over the electrolytic zone and reduces the efficiency of electrolysis. In the past, the coupled partial differential equations, describing the electromagnetic perturbation in the cell, were formulated and solved with various mathematical methods. In this article, a Fourier expansion method is used for understanding the interaction of the various non-perturbed gravity waves. A proper mathematical treatment of the boundary condition, a critical factor for solving the equations, is presented. The result is summarized as the mode interactions, governed by the symmetry of the vertical magnetic field and the symmetry of the wave modes. The dominant mechanism of the instability is explained and the various practical methods for magnetic field compensation are reviewed.

1. Introduction

In the aluminum cell, both molten electrolyte and liquid aluminum form two liquid layers in a rectangular container (Figure 1).

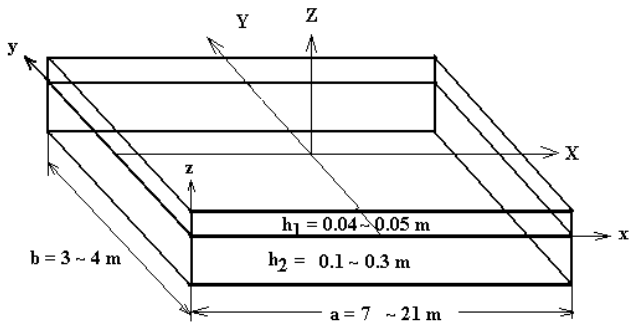

Figure 1 Container for electrolyte and liquid metal and the coordinate systems (Positive y is the direction of line current)

One coordinate system is x-y-z where the domains of x and y are [0 a] and [0 b], respectively, and the origin is located at the upstream left corner on the bath/metal surface. Another is X-Y-Z which is non-dimensional with respect to X and Y, where the domains of X and Y are both [-1 1] and the origin is in the center of the cell. The densities of the electrolyte and aluminum are around 2.1 x 10^3 and 2.3 x 10^3 kg/m^3. Thus, the electrolyte settles on the top of liquid aluminum. It has been well known that various waves occur on the interface of the layers. Such waves have been studied in many fields in science. The wave in the aluminum cell is unique because of a presence of the electromagnetic force, acting as a perturbing force to the gravity wave.

An effort to study the perturbation was intensified in 1970s and the governing equations, called "the MHD Equations" here, were presented [1] and were applied to a side-by-side arrangement as well as an end-to-end arrangement cells, having produced a good agreement with the measured waves [2]. A criteria for instability was presented [3]. A decade later, the same MHD Equations were applied to a multiple-riser cell for the metal pad stabilization [4]. Efforts in studying the waves have been carried out by many researchers and knowledge about the instability has been extended concerning traveling waves [5], widened through an inclusion of the back ground flow [6] and inclusion of the magnetic field perturbation, while mathematical understanding has been deepened ([7] and [8]). 3D modeling was also carried out ([10] and [11]). In recent years, the studies have been continued ([12],[13],[14],[26]). This article tries to study the electromagnetic perturbation from a viewpoint of mode coupling. For this purpose, first, the background assumptions are discussed, second, the analytical expression of the MHD term is derived and, third, the solutions to the equations are derived for simple yet practical cases The mechanism of the perturbation (MHD term) and the resultant instability is understood as a mode coupling between the non-perturbed gravity waves expressed by cosine functions with respect to the x-y space. The treatment of the boundary condition, which is one of the central subjects in this article, is presented.

2. MHD Equations and Assumptions

The MHD Equations consist of two coupled partial differential equations, one for electrical potential (EP Equation) and another for wave motion (WM Equation) perturbed by the electromagnetic force. The electrical resistances of the materials (Table 2.1) lead to the assumptions for the EP Equation.

Anode bus	2.7 x 10^{-8}
Anode carbon	5.0 x 10^{-5}
Electrolyte	0.5 x 10^{-2}
Liquid aluminum	25.0 x 10^{-8}
Cathode carbon	4.0 x 10^{-5}

Table 2.1 Electrical Resistance (Ohm-m)

- In calculating the electrical potentials for both electrolyte and cathode carbon, the liquid metal is assumed to be equi-potential.
- Either the anode carbon or the anode bus is assumed to be equi-potential when the electrical current in the electrolyte is calculated.
- The electrical current in the electrolyte is calculated by the resistance of the anode-to-cathode distance at each location of (x, y).

G. Bearne et al. (Eds.), *Essential Readings in Light Metals*

The assumptions for the WM equation are:

- Shallow water assumption in which the wave length λ is much larger than the depths, h_1 and h_2 of the two layers as shown below (see [15] for theory of shallow water).

(2.1) $$\lambda >> h_1,\ h_2$$

Based on these assumptions, the EP equation and its boundary conditions are

(2.2) $$(\partial_{xx} + \partial_{yy}) \varphi = - J_a \zeta /(h_1 h_2)$$

(2.3) $$\partial_{\mathbf{n}} \varphi = 0$$ at x=0 and a, also at y=0 and b.

where $\partial_{\mathbf{n}}$ is the gradient normal to the boundary.

The electrical currents are

(2.4) $$j_x = - \partial_x \varphi \qquad j_y = - \partial_y \varphi$$

where the parameters are:

φ : electrical potential (volts times σ_2) in the metal.
σ_2 : electrical conductivity of the metal (Ohm-m),
J_a : anode current density (ampere/m^2),
ζ : displacement of the bath/metal interface (upward positive) (m).
h_1 : depth of the electrolyte layer (m),
h_2 : depth of the metal layer (m),
j_x and j_y: perturbed horizontal current in the metal.

Note that ∂/∂_x and ∂/∂_y are expressed as ∂_x and ∂_y, respectively.
The WM Equation consists of terms for internal gravity waves and for the perturbation due to the electromagnetic force.

(2.5) $$M \partial_{tt} \zeta = \alpha (\partial_{xx} + \partial_{yy}) \zeta - \mathrm{div}_2 \mathbf{f}$$

Where $f_x = j_y B_z$ $f_y = - j_x B_z$,
$\mathrm{div}_2 \mathbf{f} \equiv \partial_x f_x + \partial_y f_y = j_y \partial_x B_z - j_x \partial_y B_z$.
Note that $\partial_x j_y - \partial_y j_x = 0$.

The variables are:

ρ_1 : density of electrolyte (kg/m^3)
ρ_2 : density of metal (kg/m^3)
$\delta\rho = \rho_2 - \rho_1$: difference in densities
$\alpha = \delta\rho\, g$
$M = \rho_1 / h_1 + \rho_2 / h_2$
g : gravity acceleration (m/sec^2)
B_z : z component of the unperturbed magnetic field (Gauss or Tesla, T=10^{-4} G)
$\mathbf{f}$: perturbation force

Note that the force $\mathbf{f}$ in (2.5) is defined as a difference of the horizontal forces in the metal and in the electrolyte at the electrolyte/metal boundary. Because of the continuity, or lack continuity of $\mathbf{j}$ and $\mathbf{B}$ at the boundary, only the terms involving j_x and j_y , tangential components of $\mathbf{j}$, remain in the equation.
The boundary condition is derived from the force balance at the boundary, x=0 and a, y=0 and b.

(2.6) $$\alpha \partial_{\mathbf{n}} \zeta = (n_x j_y - n_y j_x) B_z$$

When the magnetic field perturbation, a secondary effect in the perturbation, is included into the calculation, $\mathbf{j}$ is replaced with unperturbed $\mathbf{J}$, and $\mathbf{B}$ is replaced with perturbed field $\mathbf{b}$, and the new term is added to Equations (2.5), (2.6).

3. Solution

The solution of the EP and WM Equations are obtained by using the Fourier series expansion for even function.

(3.1) $$\phi_{m,n} = \varepsilon_m \varepsilon_n \cos(m\pi x/a) \cos(n\pi y/b)$$

where $\varepsilon_0 = 1/\sqrt{2}$, $\varepsilon_1 = 1$, $\varepsilon_2 = 1$, $\varepsilon_3 = 1$, ….

Thus, φ and ζ are expanded as

(3.2) $$\varphi = \sum_{m,n} \varphi_{m,n}\ \phi_{m,n}\ e^{i\omega t}$$

(3.3) $$\zeta = \sum_{m,n} \zeta_{m,n}\ \phi_{m,n}\ e^{i\omega t}$$

where $\varphi_{m,n}$ and $\zeta_{m,n}$ designate the (m,n) component of φ and ζ.

The solution of the EP Equation (2.2) is, because $\phi_{m,n}$ satisfies the boundary condition (2.3), obtained in the following.

(3.3) $$\varphi_{m,n} = \beta / \Delta_{m,n}\ \zeta_{m,n}$$

where $\Delta_{m,n} = \pi^2((m/a)^2 + (n/b)^2)$ and $\beta = J_a / (h_1 h_2)$.

Therefore, the solution for φ is written, if $\zeta_{m,n}$ is known,

(3.4) $$\varphi = \beta \sum_{m,n} (1/\Delta_{m,n})\ \zeta_{m,n}\ \phi_{m,n}\ e^{i\omega t}$$

The solution for ζ can be obtained with Galerkin method by taking into account that the Fourier component $\phi_{m,n}$ (m=0, ∞ and n=0, ∞) does not satisfy the boundary condition. Using $\phi_{m,n}$ as a trial function, Equation (2.5) is integrated over the domain.

(3.5) $$(\phi_{m,n}, M \partial_{tt}\zeta) = (\phi_{m,n}, \alpha(\partial_{xx} + \partial_{yy}) \zeta) - (\phi_{m,n}, (j_y \partial_x B_z - j_x \partial_y B_z))$$

where the inner product (f, g) is defined as $(f, g) = \iint_\Omega dx\, dy\, f^* g$.

Using Gauss-Green's Theorem, the first term on the right hand side of Equation (3.5) is

$$\alpha((\partial_{xx} + \partial_{yy})\phi_{m,n}, \zeta) + \alpha \oint_{\partial\Omega} ds\ (\phi_{m,n} \partial_{\mathbf{n}}\zeta - \zeta \partial_{\mathbf{n}}\phi_{m,n})$$

where $\partial\Omega$ is the boundary of the domain Ω of the equation.

The second term is

$$- \oint_{\partial\Omega} [\phi_{m,n}(n_x j_y - n_y j_x)B_z]ds + (\partial_x \phi_{m,n}, B_z j_y) - (\partial_y \phi_{m,n}, B_z j_x).$$

Combining two terms on the right hand side of (3.5), the final Equation becomes:

$$(3.6) \quad (\phi_{m,n}, M\,\partial_{tt}\zeta) = \alpha((\partial_{xx} + \partial_{yy})\phi_{m,n}, \zeta) + \oint_{\partial\Omega} [\phi_{m,n}(\partial_n \zeta - (n_x j_y - n_y j_x)B_z)]\,ds + (\partial_x \phi_{m,n}, B_z j_y) - (\partial_y \phi_{m,n}, B_z j_x)$$

Using the boundary condition (2.6), Equation (3.6) becomes a matrix equation for eigen-values.

$$(3.7) \quad (M\omega^2 - \alpha\,\Delta_{m,n})\,\zeta_{m,n} - \beta \sum_{m'n'} S_{(m,n),(m'n')}\,(1/\Delta_{m',n'})\zeta_{m',n'} = 0$$

for each m > 0 and n > 0 excluding the case of m=0 and n=0,

where $S_{(m,n),(m'n')}$ is

$$(3.8) \quad S_{(m,n),(m'n')} = (\partial_x \phi_{m,n}, B_z\,\partial_y \phi_{m',n'}) - (\partial_y \phi_{m,n}, B_z \partial_x \phi_{m',n'}) = - S_{(m',n'),(m\,n)}$$

The expression of the **S** matrix shows:

- Constant B_z perturbs the gravity wave.
- **S** matrix is anti-symmetric. Thus, when two modes of ω_1 and ω_2 are coupled, new $\omega_{1'}$ and $\omega_{2'}$ fall between the original ω_1 and ω_2.
- When the coupling of two modes is strong, two eigen-values become complex numbers and the wave has an exponential growth and becomes unstable.
- No coupling occurs between two longitudinal wave modes such as (m,0) and (m',0) nor between two transversal modes such as (0,n) and (0,n').

When we use 5 modes (1,0), (0,1), (2,0), (1,1), (0,2) for the Fourier expansion, non-zero elements of the **S** matrix are only eight in the upper triangle of the matrix.

	(1,0)	(0,1)	(2.0)	(1,1)	(0,2)
(1,0)	0	exists	0	exists	exists
(0,1)		0	exists	exists	0
(2,0)			0	exists	exists
(1,1)				0	exists
(0,2)					0

4. Magnetic Field and Perturbation Matrix

By using the non-dimensional coordinate system X-Y-Z, shown in Figure 1, the vertical magnetic field B_z is approximated. Two types of the distributions, that are popular among the side-by-side cells with end risers and the end-to-end cells of the conventional types, can be approximated with a simple equation.

$$(4.1) \quad B_z = Co + Cx\,X + Cy\,Y + Cxy\,XY$$

where the domains of X and Y are [-1 1] and [-1 1]. The C coefficients are dependent on the currents in the specific conductors.

Co : field due to the current in the adjacent line.
Cx : field due to the current in the cell-end cathode bus, side risers and underhung buses (bus under the cell) in side-by-side cell.
Cy : field due to the current in the cell-side cathode bus in the end-to-end cell or the anode-risers in the side by side cell.
Cxy: field due to the horizontal current in the metal, collector bar current, side cathode-ring-bus current and the current in the anode movable bus.

When the symmetry is considered for magnetic fields, the base function $\phi_{m,n}$ and its derivatives with respect to x and y, **S** matrix becomes quite simple, as follows.

$S_{(m,n),(m'n')} =$

$2/(ab)\cdot$

	(1,0)	(0,1)	(2.0)	(1,1)	(0,2)
(1,0)	0	4 Co	0	$-\sqrt{2}$ Cx	-4 Cy
(0,1)		0	4 Cx	$\sqrt{2}$ Cy	0
(2,0)			0	$16/3\cdot\sqrt{2}$ Co	4 Cxy
(1,1)				0	$16/3\cdot\sqrt{2}$ Co
(0,2)					0

Each element in the **S** matrix is closely related to the metal pad wave (cell instability) we encounter in day to day operation.

- Co, which is relatively large in the uncompensated end-to-end cells, couples the modes (1,0) and (0,1). This coupling mechanism offers an explanation to a relationship presented by Sele, who described the rotating wave crest. The superposition of (1,0) and (0,1) modes with some phase shift creates an appearance of the crest moving from one corner to another. The mechanism of coupling is shown in Figure 4.1. First, the (1,0) wave generates the horizontal current j, which, interacting with B, generates the force F in the cell width direction. This F induces the (0,1) mode as shown in the second figure. Further, the induced (0,1) mode generates the force in the length direction and enhances back the (1,0) mode to complete the interaction.

  The popular and cost-effective method of magnetic compensation has been the alteration of the current splits among 4 anode risers – see [19] for example – that reduces Co. The addition of the central risers [20] [21] tries to reduce the entire B_z.

- Cx in the coupling of (2,0) and (0,1) is related to the single most significant destabilization mechanism concerning the side-by-side cells. The mechanism of coupling is shown in Figure 4.2. (2,0) mode generates the electrical current in the length direction and, interacting with Cx component of the field, generates the (0,1) mode wave and thus generates the current in the width direction. This current, interacting with Cx, excites back the (2,0) mode.

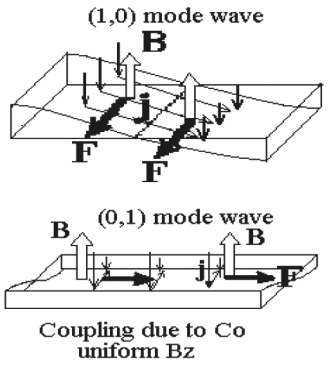

Figure 4.1

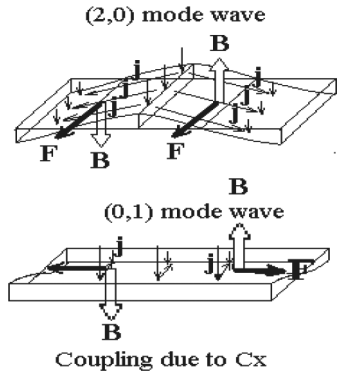

Figure 4.2

If the average B_z at each quadrant of X-Y coordinate alternates its sign when we rotate around the coordinate origin [22], Cx becomes zero. Note that the stability criteria of Cx = 0 is not same as the claims in the patent [22].

The publications that claimed or demonstrated either the reduced or zero Cx are [23].[24].[25] [26] for the side-by-side cells. Note that there are numerous patents, for new bus design of the side-by-side cells, that claimed achieving a reduced B_z, not just Cx.

- Cxy is torsional field where the sign of the field changes alternately while we rotate from one quadrant to another. Cxy is, in many cell arrangements, quite large and its effect is complex when the other C coefficients are large enough. It is noted that Cxy couples (2,0) and (0,2) modes. Because of the mode (0,2) which has a relatively short wave length, the frequency of the oscillation is high, receiving larger damping effect caused by fluid viscosity (refer to [15]).

The bus modifications and designs referred to in this section are the ones installed in a group of cells, lines or plants and limited to the ones known to the author through independent analysis or direct involvement.

5. Application to Actual Cells

Side-by-Side Arrangement Cells

The uniqueness of the magnetic field distribution depends on the anode and cathode bus positions and the current distribution in the bus. One of the examples is listed in Table 5.1. The C coefficients are for a generic end riser cell of side by side arrangement at 140 kA.

C coefficients	Co	Cx	Cy	Cxy
Values(Gauss)	10	45	0	-87

Table 5.1 C coefficients for generic end rider cell with side by side arrangement (Gauss = 10^{-4} Tesla)

Because Cy = 0, the S matrix becomes a simple sparse matrix. In the computation, the higher modes up to m + n = 8 are used and compared to the solution by finite difference method. The mesh for the finite difference approximation is 10 x 5 nodes. ρ_1 and ρ_2 are 2,100 and 2,280 kg/m^3 , respectively. h_1 and h_2 are 0.05 and 0.3 m. a and b are 7.5 and 3.0 m. The calculated result reveals that some of the eigen-values have non-zero complex part and hence these waves are unstable.

	ω_r	ω_i	T(period)
Eigen Value	0.1895	-0.036	33.160
Eigen Vector	Real part	Imaginary Part	Contribution
(1,0)	-0.045	-0.066	0.6%
(0,1)	-0.669	-0.187	48.2%
(2,0)	0.085	0.551	31.1%
(1,1)	0.180	0.234	8.7%
(0,2)	-0.008	-0.108	1.2%
(3,0)	0.219	0.054	5.1%
(2,1)	-0.105	-0.079	1.7%

Table 5.2 Unstable wave of the lowest frequency (side by side arrangement cell)

In Table 5.2, ω_r and ω_i are real and imaginary parts of the angular velocity. The contribution of each mode is shown in the fourth column. The (0,1) mode is the largest and the (2,0) mode is next largest, showing that mechanism of mutual excitation between (0,1) and (2,0) modes. The complex number of the eigen vector shows that (0,1) is advanced to (2,0) roughly by 90 degrees

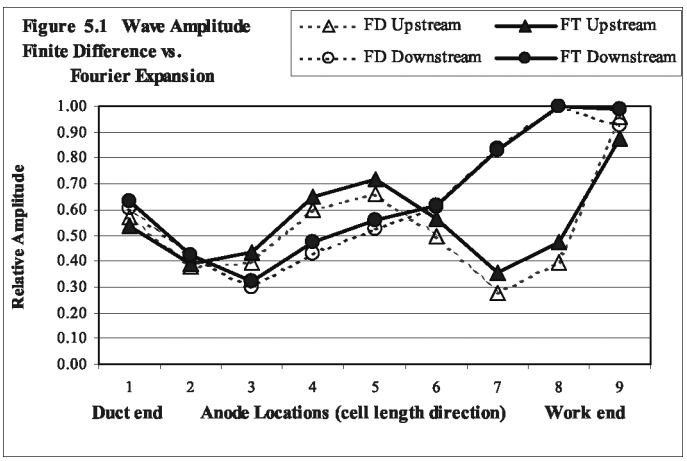

Due to phase shift between two modes, the surface contour is complicated. To compare the calculated wave to the observed wave, the displacement ζ is averaged under each anode and is plotted against the anode positions as shown in Figure 5.1

The amplitude plot agrees well with the measured anode rod currents plot. Figure 5.1 compares Fourier expansion method and Finite Difference method applied to the original equation (2.2) and (2.5). The results of both methods are close together and are expected to converge to the true solution.

A plot of the phase shift at each anode location is shown in Figure 5.2. Note that a phase shift of 1.0 is equivalent to 360 degrees.

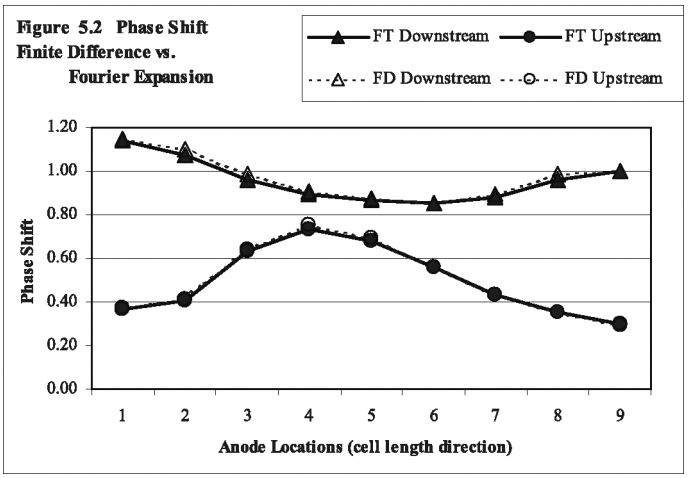

The phase shifts of non-perturbed (2,0) and (0,1) modes are shown in Figure 5.3, explaining the actual phase shift in Figure 5.2 as a mixture of the two modes. In Figure 5.3, the solid line shows the phase shift on the upstream side and dotted line, on the downstream.

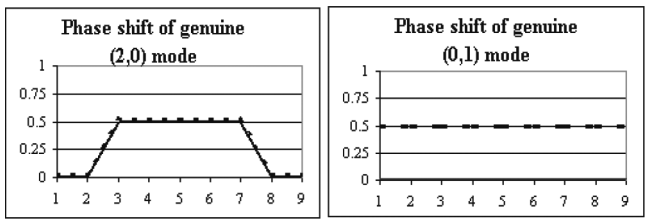

Figure 5.3 Phase shifts of gravity wave modes of (2.0) and (0,1)

Even though the (2,0) and (0,1) coupling has a clear mechanism of excitation and has been frequently observed, the mode coupling in the side-by-cell is elusive and when the interaction is intensified, other couplings, particularly the one involving the (3,0) mode is excited [27]. This mode evolution would be an interesting subject.

End-to-End Arrangement Cell

In the typical magnetically-uncompensated cells of end-to-end arrangement, Co and Cxy are dominant, as shown in Table (5.3). The values, calculated from the measured B_z [31], are slightly modified for simplicity.

C coefficients	Co	Cx	Cy	Cxy
Values(Gauss)	25	0	0	-62

Table 5.3 C coefficients for generic end-to-end arrangement cell (Gauss = 10^4 Tesla)

The amperage is 110 kA, ρ_1 and ρ_2 are 2,200 and 2,280 kg/m^3, respectively. h_1 and h_2 are 0.05 and 0.3 m. a and b are 7.0 and 2.5 m. The wave is stable at ρ_1 = 2,100 kg/m^3.

The eigen vector in Table 5.4 shows that the dominant mode is (0, 1), interacting with (1,0) and a small fraction of (3,0).

	ω_r	ω_i	T(period)
Eigen Value	0.1309	-0.047	48.0
Eigen Vector	Real part	Imaginary part	contribution
(1,0)	-0.232	0.210	9.8%
(0,1)	0.020	0.898	80.7%
(2,0)	0.000	0.000	0.0%
(1,1)	0.000	0.000	0.0%
(0,2)	0.000	0.000	0.0%
(3,0)	-0.123	-0.143	3.6%
(2,1)	0.050	-0.145	2.4%

Table 5.4 Unstable wave of the lowest frequency (end to end arrangement cell)

For the end to end cells, a stability criteria, which is equivalent to zero imaginary part in the eigen value, can be obtained from eigen matrix being approximated with the two dominant eigen modes. The result is

$$\alpha\,(\pi/2)^4\,(1/b^2-1/a^2) > J_a\,Co\,/(h_1\,h_2). \qquad (5.1)$$

With the same values of a, b, h_1, h_2 and ρ_2, the stability condition becomes $\rho_1 < 2{,}155$ kg/m^3. A lighter electrolyte, possibly with high temperature and/or low excess aluminium fluoride, makes the metal more stable. Equation (5.1) is a derivation of the stability criteria by Sele (see also [6] and [9]). In the same way, a stability criteria for the side by side cell will be expressed mainly by Cx instead of by Co.

The analysis of the magnetically compensated and/or large amperage cells needs to involve the higher modes such as m=4 to 7 modes [27][28]. Even in such cells, Cx = 0 is still crucial [29]. A 300 kA cell with a large Cx was reported to be very unstable (Figure 4 in [28]). A wave in a 200 kA cell reported in [30] appears containing (2,0) and (0,1) modes, similar to those reported in [4].

6. Solution Methods

A publication[12] questioned the validity of the Fourier expansion method for solving the MHD equation. The reason of the questioning was that the derivative of cosine is zero at the boundary and hence the solution consisting of cosine series cannot satisfy the boundary condition. Figure 5.1 demonstrates, however, that the solutions obtained by two methods agree each other, showing that Fourier method is valid. Regarding the question about the derivative at the boundary, the Jordan-Lebesques Theorem about uniform convergence of Fourier series assures the convergence of the series to the solution at (0,a), excluding at point 0 and a, whose measures(areas) are zero. Regarding the convergence to the true solution, it should be noted that the derivation process, leading to Equation (3.7), employed a weak form of the partial differential equation. The convergence was proven in the works in Functional Analysis such as developed in [16] and [17]. However, this validity question points out an

importance of handling the boundary condition. When the boundary condition is neglected and the perturbation matrix is calculated, the solution leads to an entirely wrong stability criteria, possibly nullifying the bus design effort. Note also that solving the partial differential equations, by using trial functions that do not satisfy the boundary condition, has been well studied in the area of finite element method. Instead of the intuitive derivation shown here, one can refer to [18], that gives the same result derived here.

7. Conclusion

1. Three decades ago, a MHD equation was presented and solved for the motion of the metal pad in both the side-by-side and the end-to-end cells and later re-applied to the 190 kA cell. The wave study was enriched and broadened by many researchers. This article discussed the interaction in terms of mode coupling.
2. The correct solution was obtained by using a Fourier expansion together with a Galerkin method, which can produce the correct solution in cases where the trial function does not satisfy the boundary condition.
3. Fourier expansion method clarified the electromagnetic interaction of the genuine gravity waves. The obtained perturbation matrix has an anti-symmetric nature and is sparse due to symmetry of B_z, j_x and j_y, and therefore offered a clear view of the perturbation. The analytical expression of the perturbation matrix was calculated up to the 5^{th} mode.
4. The metal pad in the side-by-side arrangement cell tends to destabilize due to Cx, gradient of B_z in the cell length direction, and generates a mode coupling of (2,0) and (0,1). The metal pad in the end-to-end arrangement cell tends to destabilize due to Co, constant B_z, and generates a mode coupling of (1,0) and (0,1).
5. The criteria for stability presented by Sele was derived from the MHD equation. The rotating crest reported in his paper was explained from the mode coupling of (1,0) and (0,1).

References

1. K. Mori, K. Shiota, N. Urata and H. Ikeuchi. The Surface Oscillation of Liquid Metal in Aluminium Reduction Cells. Light Metals Vol. 1 1976 pp 77-95.
2. N. Urata, K. Mori and H. Ikeuchi. Behavior of Bath and Molten Metal in Aluminum Electrolytic Cell. Keikinzoku (Light Metals Japan) Vol. 26, No.11, 1976, pp 573.
3. T. Sele. Instability of the Metal Surface in Electrolytic Alumina Reduction Cells. Met.Trans. B, Vol 8B, 1977, pp 613-618.
4. N. Urata. Magnetics and metal pad instability. Light Metals 1985 pp 581-589.
5. R. Moreau and D. Ziegler. Stability of Aluminum Cells – A New Approach. Light Metals 1986 pp 356-364.
6. D. P Ziegler. Stability of Metal/Electrolyte Interface in Hall-Heroult Cells: Effect of the Steady Velocity. Met.Trans. B, Vol 24B, 1993, pp 899-906.
7. V. Bojarevics and M. V. Romerio, Long wave instability of liquid metal-electrolyte interface in aluminum electrolysis cells: a generalization of Sele's criterion. Eur. J. Mech. B/Fluids, 13,(1994), pp 33-56.
8. D. Sneyd and A. Wang. Interface instability due to MHD mode coupling in aluminum reduction cells, J. Fluid Mech., 263 1994 pp 343-359.
9. P. A. Davidson and R. I. Lindsay, Stability of interfacial waves in aluminum reduction cells, J. Fluid Mech., 362, 1998, pp 273-195.
10. V. Potcnik. Modelling of Metal-Bath Interface Waves in Hall-Heroult Cells using ESTER/PHEONICS. Light Metals 1989 pp 227-235.
11. M. Segatz and C. Droste. Analysis of magneto-hydrodynamic instabilities in aluminium reduction cells. Light Metals 1994 pp 313-322.
12. C. Droste, M. Segatz and D. Vogelsang. Improved 2-Dimensional Model for Magnetohydrodynamic Stability Analysis in Reduction Cells. Light Metals 1998 pp 419-428.
13. K. Kalgraf. Stability of Hall-Heroult Cells. Light Metals 2001 pp 427-432.
14. Wu Jiankang and Huang King, Finite Element Analysis of Magnetohydrodynamics Stability of an Aluminum Reduction Cell. Light Metals 2002 pp 511-514.
15. L. Landau and E. Lifshits, Fluid Mechanics Pergamon Press 2nd English, rev. edition. 1987
16. L. Schwartz. Théorie des Distributions. Hermann & Cie. Paris.
17. K. Yoshida. Functional Analysis. Springer-Verlag Berlin Heidelberg 1995
18. O.C. Zienkiewicz and R. L. Taylor. The Finite Element Method. Fourth Edition Vol.1. Chapter 9 McGraw-Hill 1994.
19. K. Paulsen, W. Rolland, T.B.Svendson and M. Bugge. Factors Explaining the Improvements in Performance in the Soederberg Lines at Hydro Aluminium Karmoy. TRAVAUX Vol. 23 1996 No. 27 pp 301.
20. B. Langon. Breakthrough in Prebake and Soederberg End-to-end Pots. Light Metals. 1980 pp 391-400.
21. T. Johansen, H. Petter and R. Kaenel. Productivity Increase at Soeral Smelter. Light Metals. 1999. pp 153-170.
22. P. Morel and J.P. Dugois. UK Patent Application GB 2021 647 A May 24 1979. Fig. 4.
23. G. Newsted, H. Meyer, R. Hawkins and J. Johnson. Twenty five years of progress at Intalco. Light Metals 1992 pp 307.
24. G. E. da Mota, G. J. de Andrade. Magnetic Compensation Project at Albras Smelter. Light Metals. 2001 pp 413-418
25. G. Degan. Use of Iron Shields for Correcting Local Disturbance of Magnetic Fields in the electrolytic Pots. Light Metals 1986. pp 551-554.
26. A. Panaitescu, A. Moraru and I. Panaitescu. Research on Instabilities in the Aluminum Electrolysis Cell. Light Metals 2003 pp 359-306.
27. H. Tang and N. Urata. Metal Pad Wave Analysis Using Fast Anode Lowering Method. Light Metals 1997 pp 387-394
28. A.S. Derkach and A.P. Skvortsov. Experience of Development and Implementation of Super High Intensity Prebake Cells (More than 250 kA). Aluminium of Siberia – 99 pp 20-32
29. R. Zabreznik and E. Tarapore. Development of the Kaiser Aluminum 195 kA Cell. Light Metals 1984 pp 455-473.
30. G. Bearne, M. Dunn, M. Roberts and Y. Mohammed. The CD200 Project – The Development of a 200 kA Cell Design From concept to Implementation. Light Metals 1997 pp 243-245.
31. N. Urata, Y. Arita and H. Ikeuchi. Magnetic Field and Flow Pattern of Liquid Aluminum in the Reduction Cells. Light Metals 1975 pp 233-249.